Journal of Materials Science: Materials in Electronics (2020) 31:8394–8402
https://doi.org/10.1007/s10854-020-03374-y

Li-ion battery cathode performance from the electrospun binary $LiCoO_2$ to ternary $Li_2CoTi_3O_8$

Özlem Kap[1] · Alper Inan[2] · Mesut Er[3] · Nesrin Horzum[1]

Received: 27 December 2019 / Accepted: 7 April 2020 / Published online: 13 April 2020

Abstract

Metal oxide nanofibers are prepared by electrospinning and are developed to be the electrodes for lithium-ion batteries (LIBs). The effect of calcination temperature and the Li:Co mole ratio of $LiCoO_2$ nanofibers was investigated on the electrochemical cathode performance in a coin cell battery. The higher temperature calcination and Li:Co mole ratio have improved the electrochemical performance of the nanofibers. Lithium cobalt oxide ($LiCoO_2$) nanofibers obtained at 400 and 700 °C retain 65% and 90% of the initial capacity, respectively, after the high-current test and the C-rate reverted to 0.1 C. When doubling the mole ratio of Li:Co (2:1), an increase in specific capacity values from 78 to 148 mAh g^{-1} has been provided. Additionally, colloidal titania nanoparticles (TiO_2 NPs)-doped $LiCoO_2$ nanofibers were obtained and investigated as a cathode material. While the increment in calcination temperature results in higher crystallinity and stability of the $LiCoO_2$ phase, in the presence of the TiO_2 NPs causes a transformation of binary ($LiCoO_2/TiO_2$) to ternary Li-based transition metal oxide ($Li_2CoTi_3O_8/TiO_2$). An initial discharge capacity of 82 mAh g^{-1} was found at 0.1 C for the $Li_2CoTi_3O_8/TiO_2$ nanoparticles and the capacity retention was 83% when returned to 0.1 C after 25 cycles.

1 Introduction

Due to the exponential increase in the use of portable electronic devices and electric vehicles in recent years, the demand for power by electronics has created a great interest into the research and development of advanced rechargeable battery systems [1–3]. Li-ion batteries (LIBs) are one of the most significant energy storage battery systems due to its many benefits such as higher energy density, longer cycle life, and higher voltage compared to other rechargeable batteries (e.g., lead-acid, Ni–Cd batteries) [4]. Basically, LIBs consist of an anode, a cathode, and an electrolyte containing a dissociated lithium salt. For the production of LIBs with superior electrochemical properties, the type of materials used as the components play an important role [5, 6]. In recent reports, polymers are often used as the electrolytes, while transition metal oxides are commonly used as the active cathode and anode materials, due to their flexibility, and availability for the use in microsystems [7]. The most commonly used metal oxides for the cathode in LIBs are $LiCoO_2$ [8], $LiNiO_2$ [9], and $LiMn_2O_4$ [10], for the anode $LiFeO_2$ [11] and $Li_4Ti_5O_{12}$ [12, 13] are used. Among the listed cathode materials, $LiCoO_2$ is the most popular choice for microscale technologies such as mobile phones and laptops due to its high specific energy, long life cycle, and ease of production. Although it has an excellent cycle ability at room temperature, the specific capacity of the metal oxide is limited by approximately 139 mAh g^{-1} whereas the theoretical capacity is 273 mAh g^{-1}. These limitations arise from the slow diffusion of lithium cations [14, 15]. A research on the crystal chemistry and physical properties of lithium complexes has been conducted by Kawai et al., that showed $Li_2CoTi_3O_8$ has the higher reactivity among ternary titanium complexes due to the cation distributions that arising from the change in symmetry with the increase in temperature [16]. TiO_2, which has a high specific capacity of 335 mAh g^{-1}, is preferred as a doping material because

Electronic supplementary material The online version of this article (https://doi.org/10.1007/s10854-020-03374-y) contains supplementary material, which is available to authorized users.

✉ Nesrin Horzum
nesrin.horzum.polat@ikc.edu.tr

[1] Department of Engineering Sciences, İzmir Kâtip Çelebi University, 35620 Çiğli, İzmir, Turkey

[2] Department of Materials Science and Engineering, Izmir Institute of Technology, 35430 Urla, İzmir, Turkey

[3] Tübitak Marmara Research Center Energy Institute, 41470 Gebze, Kocaeli, Turkey

it controls the fiber morphology and increases the specific capacity due to its high conductivity [17, 18]. Therefore, the stable skeleton provides high capacity with bimetallic structures that facilitate the transfer of electrons [19].

The electrode materials at the microscale and nanoscale have attracted attention for LIBs owing to their fast transport of Li^+ ions by a shorter diffusion path and a high mass/charge ratio. Therefore, LIBs might be much safer and have a faster solid-state diffusion [20, 21]. Particularly, nanofibers provide a much lower charge transfer resistance between the electrolyte and the electrode materials [22, 23]. Nanofibers can be easily generated on a large scale by electrospinning with the diameter ranging from hundred nanometers or less to several micrometers [24]. The cost-effective technique provides simplicity in production and allows to fabricate structural features such as high surface-to-volume ratio, inter-fiber porosity, and interconnectivity which are advantageous for the diffusion of molecules or ions [25, 26]. Due to these properties of electrospun nanofibers, it is known that they will contribute to the performance of the battery by being a structural framework to nanoparticles, which makes them a unique candidate for battery applications [27].

In the present work, $LiCoO_2$-based nanostructures were fabricated using different calcination temperatures and Li:Co mole ratios, and using TiO_2 colloidal nanoparticles. We particularly focused our attention on which route does a positive performance change on the lithium cobalt oxide material as a cathode electrode. Since the cathode material is a limiting factor on the capacity of the batteries, the cathode performance of $LiCoO_2$ nanofibers was examined in terms of not only the effect of calcination temperature but also the effect of a variable amount of the Li^+ precursor. Moreover, $Li_2CoTi_3O_8$ nanofibers, which were obtained at higher calcination temperature by adding colloidal TiO_2 nanoparticles to the polymer solution, were investigated to compare the structural conversion from binary $LiCoO_2$ to ternary $Li_2CoTi_3O_8$ on the battery performance.

2 Experimental

2.1 Materials

Lithium hydroxide monohydrate (Aldrich, 98%), cobalt (II) hydroxide (Aldrich, 95%), poly(acrylic acid) (PAA, $M_w = 450{,}000$ g mol^{-1}, Aldrich), *N*-methyl-2-pyrrolidone (NMP, Merck), polyvinylidene fluoride (PVDF, Alfa Aesar), carbon super P (TIMCAL), 1 M lithium hexafluorophosphate $LiPF_6$ (Aldrich, 50/50 (v/v) in ethylene carbonate/diethylene carbonate (EC/DEC), colloidal TiO_2 (a mixture of rutile and anatase nanoparticles < 150 nm particle size (volume distribution, DLS), 33–37 wt% dispersion in H_2O, Aldrich) were used without further purification. Demineralized water was used throughout the study.

2.2 Preparation of electrospinning solutions

The electrospinning solutions were prepared as previously reported [28]. Briefly, LiOH was added to an 11 wt% aqueous solution of PAA (0.870 g) and stirred for 1 h at room temperature. $Co(OH)_2$ was dissolved in 3 mL of H_2O and was added into a LiOH/PAA solution to prepare a solution with a Li:Co mole ratios of 1:1 and 2:1. The mixture was stirred for 1 day at room temperature. For the fabrication of the TiO_2 containing PAA/metal salts solution, the TiO_2 NPs were dispersed in 4.0 g of the PAA/Li and Co salts solution. The weight ratio of PAA:TiO_2 was fixed at 1:1.

2.3 Fabrication of electrospun nanofibers

The electrospinning process was performed with a commercial platform (Inovenso Basic Setup). The precursor solutions of PAA/LiOH/$Co(OH)_2$ or PAA/LiOH/$Co(OH)_2$/TiO_2 were injected into a plastic syringe connected with a polyethylene tubing. The feed rates of the solutions were adjusted to 1.0 and 1.5 mL h^{-1} by a microinfusion pump. The applied voltage and tip-to-collector distance were set to 13–15.5 kV and 18–19 cm. PAA/LiOH/$Co(OH)_2$ and PAA/LiOH/$Co(OH)_2$/TiO_2 composite nanofibers were subjected to calcination under air by a muffle furnace (Protherm, PLF/20/27, Turkey) in two steps. In the first step, the nanofibers were calcinated at 400 °C with a rate of 4 °C min^{-1} for 5 h. In the second step, the obtained inorganic nanofibers were further calcinated at 700 °C for 8 h with a rate of 5 °C min^{-1}.

2.4 Characterization

The thermal behavior of the composite nanofibers was characterized by thermogravimetric analysis (TGA, Perkin Elmer Diamond TG/DTA) at a heating rate of 10 °C min^{-1} under air. Morphological images of the nanofibers were examined by scanning electron microscope (SEM, Philips XL 30S FEG and FEI QUANTA 250 FEG). X-Ray diffraction (XRD) patterns of the nanofibers were recorded in a Philips X'Pert Pro diffractometer.

2.5 Electrochemical measurements

The electrodes were prepared by mixing of active materials, carbon super P (TIMCAL) and PVDF (Alfa Aesar) with a weight ratio of 80:10:10 (%) into the solvent, 0.7 mL *N*-methyl-pyrrolidone (NMP). Lithium metal oxide nanostructures were kept for 1 h at 130 °C in the oven to minimize water adsorption. The electrode additives and 80 mg of lithium metal oxide nanostructures were mixed

for 30 min in a planetary ball mill (Fritsch Pulverisette 6). The slurry was coated on a 1.5 cm^2 aluminum disk and dried for 2 h at 85 °C in a vacuum. The disk was hot-pressed at 90 °C with a pressure of 300 kg/cm^2. Electrodes were dried in vacuum at 125 °C for 1 h and then pressed coin cells (CR2032) were prepared under an argon atmosphere in a glove box (Vigor SG 2400/1000). Lithium metal served as the anode and a 1 M solution of $LiPF_6$ was used as the electrolyte (w/w 1:1 EC:DEC). Cyclic voltammetry measurements were performed with an EL-Cell 3-electrode electrochemical cell by using lithium as a counter and reference electrode and a prepared electrode as a working electrode by using Princeton Applied Research VersaSTAT MC analyzer system. The voltage range was between 0–4.5 V at a scan rate of 0.1 mV s^{-1}.

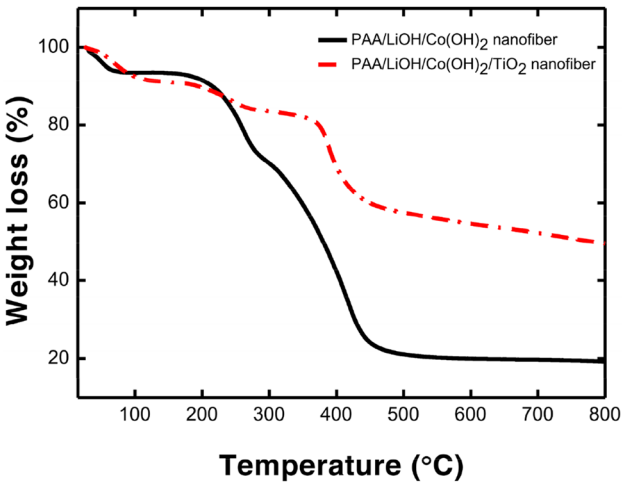

Fig. 1 TGA curve of electrospun PAA/LiOH/$Co(OH)_2$ and PAA/LiOH/$Co(OH)_2$/TiO_2 nanofibers

3 Results and discussion

$LiCoO_2$ nanofibers and TiO_2 supported $LiCoO_2$ nanofibers were fabricated by electrospinning from aqueous solutions of PAA, lithium cobalt hydroxides, and TiO_2 colloids followed by controlled heat treatment of the composite nanofibers. PAA was selected as the sacrificial polymer carrier and binder in the fibers because it is an electrospinnable polyelectrolyte, with most of the carboxyl groups being deprotonated at neutral pH providing the ability to coordinate metal cations [29–31]. TiO_2 NPs were used because of their nontoxicity and stability [32, 33].

The thermal behavior of the PAA/LiOH/$Co(OH)_2$ and PAA/LiOH/$Co(OH)_2$/TiO_2 nanofibers was conducted by using TGA. Figure 1 shows the thermograms of the composite nanofibers to determine if PAA was removed after heat treatment. The first weight loss belongs to the evaporation of volatile species at 85 °C. The second decomposition starts at 100 °C and results from the conversion of metal salts to metal oxides with the removal of the PAA backbone. There is no significant weight change detected after 430 °C indicating that the formation is completed for $LiCoO_2$ [28]. The reaction for PAA/LiOH/$Co(OH)_2$/TiO_2 nanofibers continues up to 700 °C. The further weight loss is responsible for the formation of $Li_2CoTi_3O_8$ where the thermal stability and decomposition temperature increase in the presence of TiO_2 colloids. The remaining amount of inorganic material is 19% and 47% for calcinated PAA/LiOH/$Co(OH)_2$ and PAA/LiOH/$Co(OH)_2$/TiO_2 nanofibers, respectively. TGA analysis proved the chemical compositional change, providing critical information on the calcination temperature profile; therefore, 400 °C and 700 °C were chosen as the calcination temperatures to obtain metal oxide nanofibers. Elemental analysis by energy-dispersive X-ray (EDX) spectroscopy also indicated the presence of cobalt, oxygen, and titanium in the hybrid fibers, which is attributed to the formation of $LiCoO_2$ and $Li_2CoTi_3O_8$/TiO_2 nanofibers (Fig. S1).

The morphological characterization of the nanofibers was obtained by SEM. Figure 2a, b display the low and high magnification SEM micrographs of the PAA/LiOH/$Co(OH)_2$ nanofibers before calcination. The surfaces of the nanofibers are smooth and uniform in their diameters ranging from 375 to 485 nm without any beads. The decomposition of the lithium/cobalt hydroxides and PAA occurred upon calcination at 400 °C. $LiCoO_2$ nanoparticles (28 ± 7 nm) nucleated on the surface of the nanofibers. The average fiber diameter was 350 ± 50 nm (Fig. 2c, d). After increasing the calcination temperature to 700 °C, the diameter of the fibers decreased down to 320 ± 55 nm, and the diameter of the nanoparticles was 67 ± 17 nm indicating that most of the polymer was removed. $LiCoO_2$ nanostructures were still found to preserve the fiber morphology (Fig. 2e, f). The particle size distributions of $LiCoO_2$ estimated from SEM micrographs are given in Fig. S2. It was observed that the particle size increases at higher calcination temperatures due to the grain growth [34]. In addition, the higher calcination temperature lead to the higher surface area of nanofibers by decreasing the fiber diameter [35].

The crystal structures of the $LiCoO_2$ nanofibers obtained by calcinating at 400 °C and 700 °C were examined by XRD (Fig. 3). The diffraction patterns correspond to the (003), (101), (012), (104), (015), (107), (018), (110), and (113) crystal planes which are the characteristic signals of a rhombohedral $LiCoO_2$ structure, and at $2\theta = 31°$, 55° indicate a small amount of Co_3O_4. The intensity of the $LiCoO_2$ nanofibers calcinated at 700 °C is slightly higher than the nanofibers calcinated at 400 °C, indicating the higher crystallinity with an increase in the calcination temperature. The sizes of the crystallites estimated by the Scherrer equation

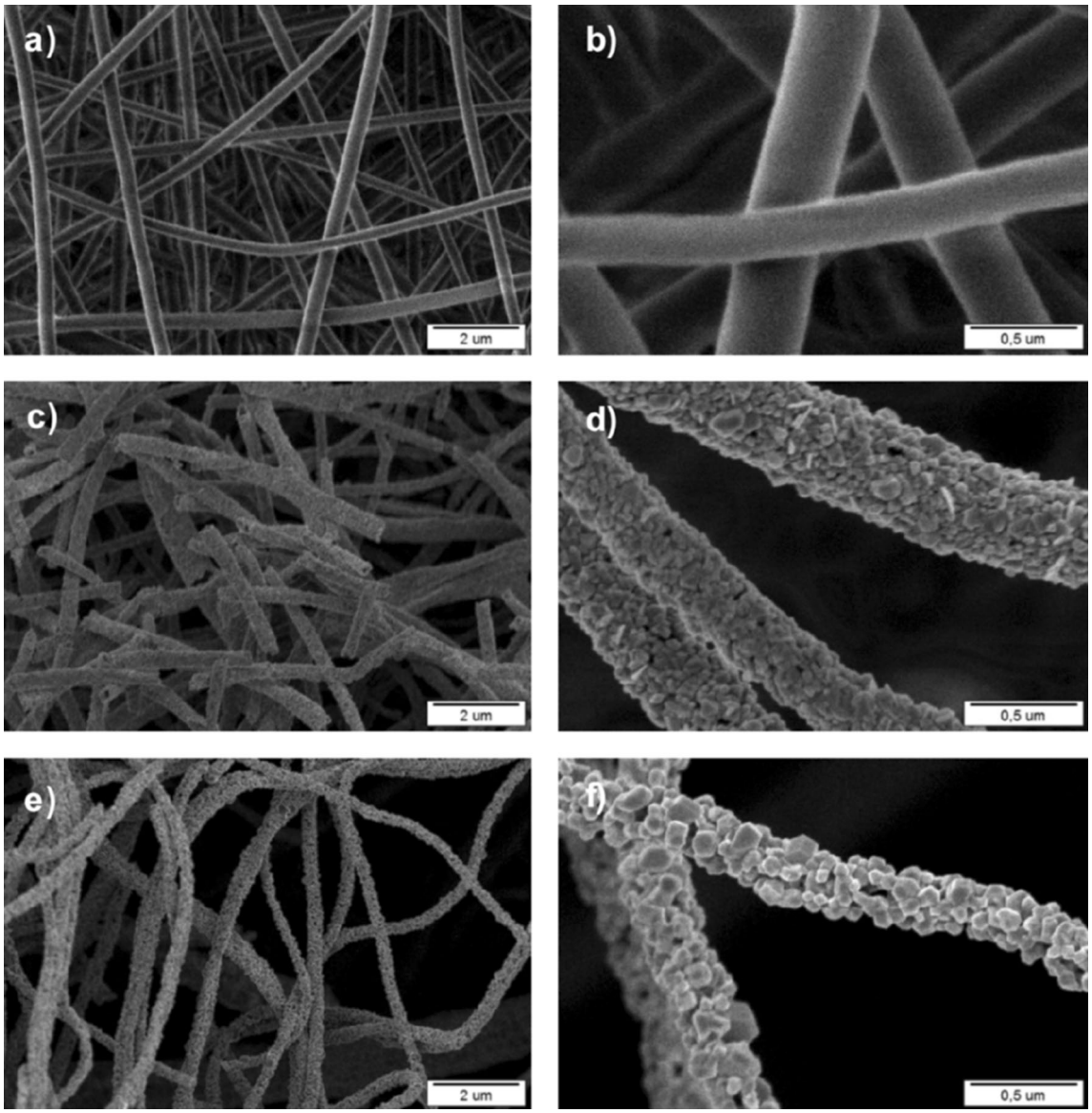

Fig. 2 **a**, **b** SEM micrographs of PAA/LiOH/$Co(OH)_2$ nanofibers before calcination; **c**, **d** after calcination at 400 °C for 5 h; **e**, **f** after calcination at 700 °C for 8 h

[36] from (104) reflection are 16 and 35 nm for $LiCoO_2$ nanofibers calcinated at 400 °C and 700 °C, respectively.

Figure 4a shows the SEM micrograph of PAA/LiOH/$Co(OH)_2$/TiO_2 nanofibers. TiO_2 colloids are homogeneously dispersed into the PAA/LiOH/$Co(OH)_2$ nanofibers with a diameter of 490 ± 50 nm which are observed as light-colored regions. After controlled heat treatment up to 400 °C, $LiCoO_2$/TiO_2 nanofibers were formed, the diameters of the nanofibers varied around 380 ± 80 nm (Fig. 4b). Further increasing the calcination temperature to 700 °C led to the formation of lithium cobalt titanate ($Li_2CoTi_3O_8$)/TiO_2 interconnected nanoparticles; however, the fiber morphology was lost. While the color of $LiCoO_2$/TiO_2 nanofibers is dark gray, $Li_2CoTi_3O_8$/TiO_2 nanostructured powder has a green color, which consists of the nanoparticles with the average diameter of 100 ± 20 nm (Fig. 4c). Wang et al. reported on the bluish-green $Li_2CoTi_3O_8$ powder which was composed of particles with a size around 100–200 nm prepared by a simple citric nitrate method [37].

XRD patterns of $LiCoO_2$/TiO_2 nanofibers obtained at different calcination temperatures are shown in Fig. 5. While the crystal structure of the nanofibers obtained at 400 °C is composed of rhombohedral $LiCoO_2$ and tetragonal TiO_2, at 700 °C is transformed into cubic $Li_2CoTi_3O_8$ and tetragonal TiO_2 nanoparticles. In the presence of TiO_2 colloids, the crystallite size of $LiCoO_2$ is calculated as 24 nm from the

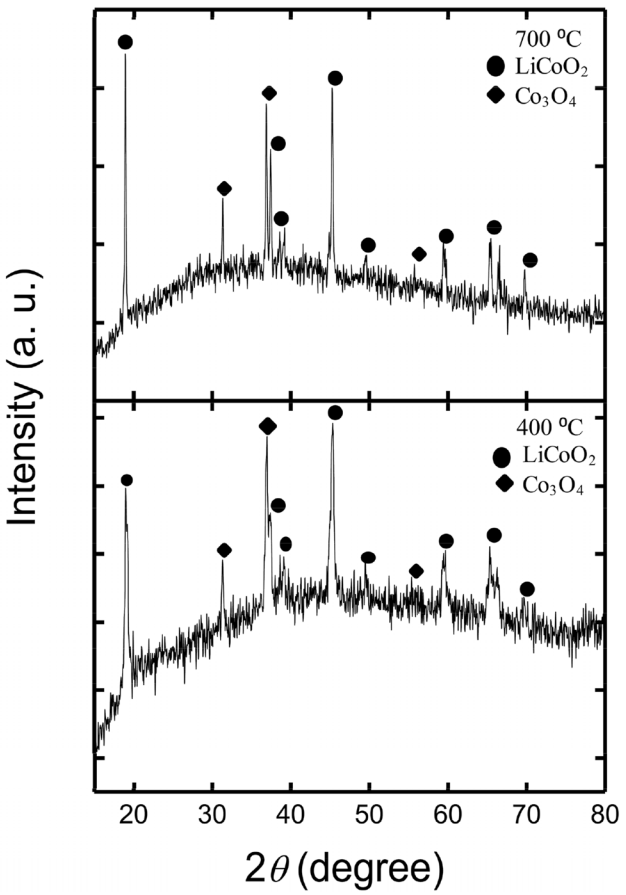

Fig. 3 XRD pattern of $LiCoO_2$ nanofibers obtained at 400 °C and 700 °C

(200) at 400 °C and $Li_2CoTi_3O_8$ is calculated as 40 nm at 700 °C from the (110) reflection.

Figure 6a shows the results of the discharge capacity tests of $LiCoO_2$ cathode electrodes synthesized with a mol ratio of 1:1 (Li:Co), which are heat-treated at 400 and 700 °C at a discharge rate ranging from 0.1 to 2.0 C-rates for 5 cycles. In the first cycle at 0.1 C, a discharge capacity of 62 mAh g^{-1} was found for the 400 °C heat-treated $LiCoO_2$ nanofiber, whereas the capacity of the 700 °C heat-treated $LiCoO_2$ cathode material was 78 mAh g^{-1}. Although the charge capacities between the materials seem close to each other, the different trend was observed in the following cycles. The capacity dropped dramatically for 400 °C heat-treated nanofibers for each 5 cycles, namely, 30 mAh g^{-1} at 0.5 C, 25 mAh g^{-1} at 1.0 C, 18 mAh g^{-1} at 2.0 C. The specific capacity was measured to be around 40 mAh g^{-1} when the battery discharged again at 0.1 C. On the contrary, the capacity for 700 °C heat-treated nanofibers were measured to be more stable in comparison to the 400 °C heat-treated nanofibers for each 5 cycles, namely; 63 mAh g^{-1} at 0.5 C, 58 mAh g^{-1} at 1.0 C, and 36 mAh g^{-1} at 2.0 C. The capacity of the material was recovered

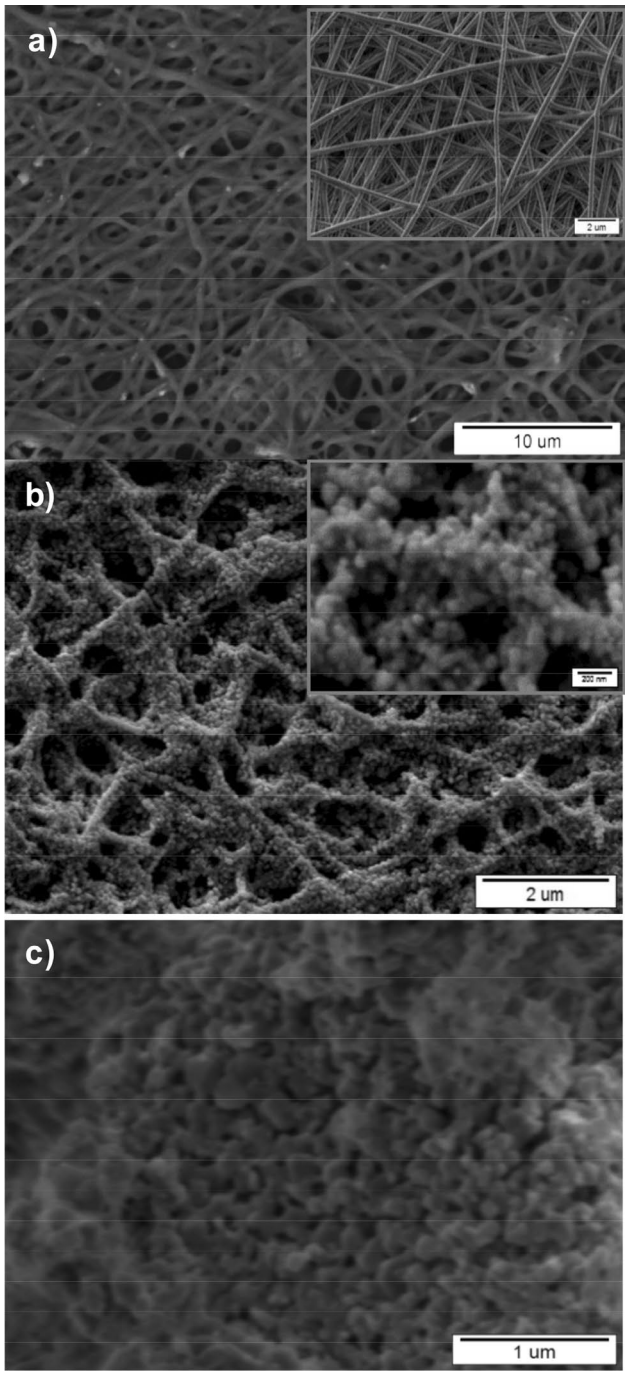

Fig. 4 SEM micrographs of **a** PAA/LiOH/$Co(OH)_2$/TiO_2 nanofibers before calcination, **b** $LiCoO_2$/TiO_2 nanofibers obtained at 400 °C for 5 h calcination, **c** $Li_2CoTi_3O_8$/TiO_2 obtained at 700 °C for 8 h calcination

after returning to 0.1 C (70 mAh g^{-1}) indicating that 90% of the initial capacity was retained after 20 cycles. Thus, after testing with different C-rates between the two samples, it can be concluded that higher temperature heat treatment increases the stability of the coin cell battery and the surface area of the active material. As a result of

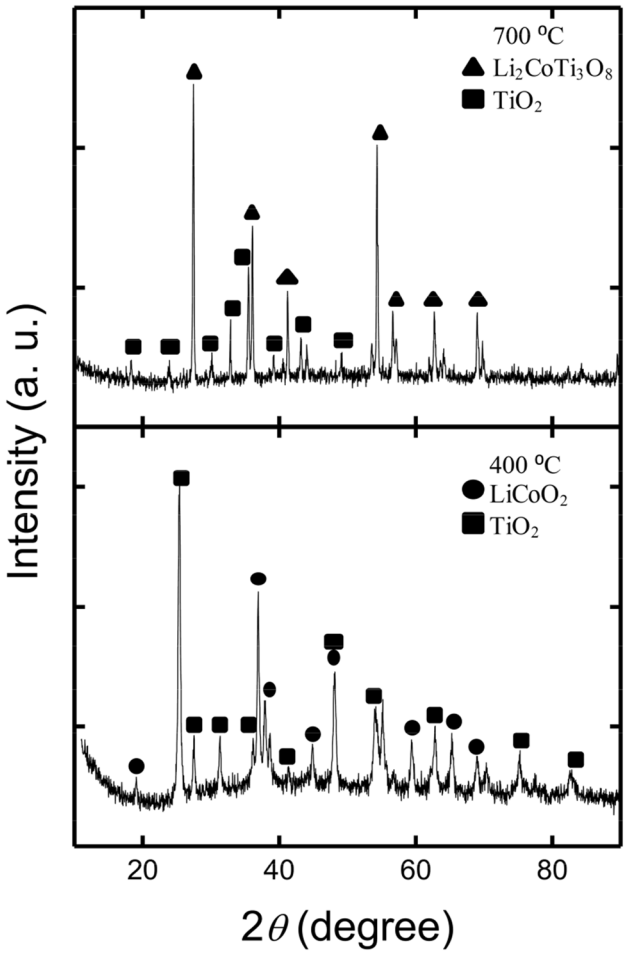

Fig. 5 XRD pattern of the $LiCoO_2/TiO_2$ nanofibers obtained at 400 °C and $Li_2CoTi_3O_8/TiO_2$ nanofibers obtained at 700 °C

the existence of more accessible areas, a higher capacity cycle has been achieved by more lithium-ion insertion/deinsertion [38].

The cyclic voltammetry curve of $LiCoO_2$ nanofibers fabricated at 700 °C is given in Fig. 6b at a scanning rate of 0.1 mV/s and between 2.5–4.5 V. Delithation/lithiation peaks appeared noticeably at the potentials 3.96 V and 3.86 V, indicating the transfer of lithium ions from the intercalation sites into the $LiCoO_2$ and deintercalation out of the $LiCoO_2$ structure of lithium ions to lithium anodes during anodic and cathodic sweeps, respectively. Additionally, less prominent peaks resulting from order/disorder phase transitions were observed at 4.19 V and 4.15 V.

Evaluating the cathode performance of the charge and discharge profiles of $LiCoO_2$ nanofibers calcinated at 700 °C were tested, as shown in Fig. 6c. The charge capacity of the battery was observed to be 94 mAh g^{-1} whereas the discharge capacity was 78 mAh g^{-1}. A charge potential plateau was detected, which corresponds to the Li extraction and insertion potentials at 3.80 and 3.90 V, respectively. The

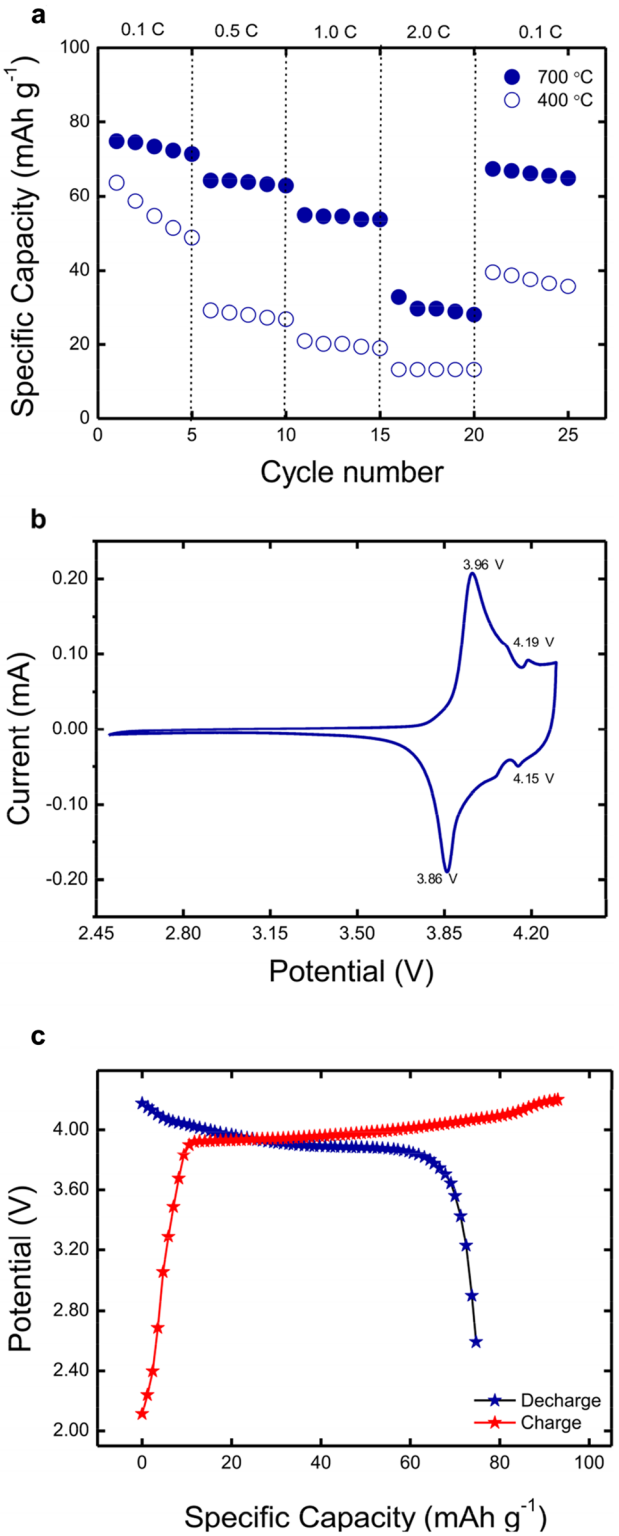

Fig. 6 **a** Rate performance of $Li/LiCoO_2$ coin cell battery ($LiCoO_2$ nanofibers were fabricated at 400 °C and 700 °C with a Li:Co mole ratio of 1:1). **b** Cyclic voltammogram of $Li/LiCoO_2$ coin cell battery at scan rate of 0.1 mV/s. **c** Charge–discharge curve of $Li/LiCoO_2$ coin cell battery

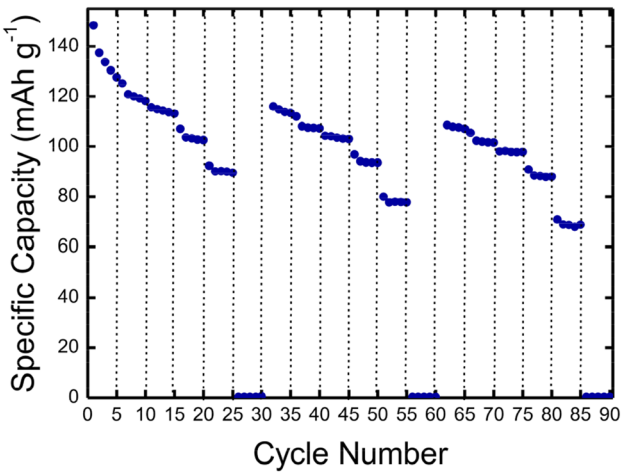

Fig. 7 Rate performance of Li/$LiCoO_2$ coin cell battery ($LiCoO_2$ nanofibers were fabricated at 700 °C with a Li:Co mole ratio of 2:1)

initial coulombic efficiency was obtained as 80% for the Li/$LiCoO_2$ coin cell battery.

To achieve an enhancement on battery performance due to the higher insertion of lithium into the crystal structure of $LiCoO_2$, a modification has been applied to the nanofiber fabrication changing the Li:Co mole ratio. Figure 7 shows the rate performance of $LiCoO_2$ nanofibers with a Li:Co mole ratio of 2:1. A 90 charge/discharge cycle testing was performed at the following rates: 0.2, 0.5, 1.0, 2.0, 4.0, and 10 C for each 5 cycles. An initial discharge capacity of 148 mAh g^{-1} was found at 0.2 C for the $LiCoO_2$ nanofibers. The capacity faded to 120 mAh g^{-1} at 0.5 C, 118 mAh g^{-1} at 1.0 C, 108 mAh g^{-1} at 2.0 C, 91 mAh g^{-1} at 4.0 C. No capacity was observed at the high C-rate (10 C) [39]. The decrease in the capacity after each 30 charge/discharge cycles is 20% and 8% for the nanofibers. The higher cycle capacity was obtained when the Li:Co mole ratio doubled in $LiCoO_2$ nanofibers. The increased amount of lithium enhanced the electrical conductivity of the electrode in the crystal lattice [40]. Ou et al. investigated the effect of different calcination temperatures and La_2O_3 coating on the discharge capacities and cyclic stability of $LiCoO_2$ powders derived from electrospun nanofibers [41]. Although these trials do not change the discharge capacity that much, it was shown that after the 30 cycles, the retention of the initial capacity of the $LiCoO_2$ powders was increased from 76 to 84% at higher calcination temperature, while in the case of additional surface modification with La_2O_3 was further increased to 91%. In a similar study, Mizuno et al. clarified the electrochemical properties of wire-structured $LiCoO_2$ by adding vapor-grown carbon fiber (VGCF) into the precursor solution [42]. On the one hand, VGCF led to obtaining thinner $LiCoO_2$ fibers which were resulted in an initial capacity of 137 mAh/g with 35% loss after 30 cycles. On the other hand, the initial capacity for bare $LiCoO_2$ was 135 mAh/g with 20% loss after 30 cycles. This capacity fade occurred on the VGCF fiber was explained by the surface resistive layer due to the irreversible electrochemical reaction at the initial cycles.

To examine the electrochemical properties of $Li_2CoTi_3O_8$/TiO_2 in a half cell configuration as a cathode material for LIBs, a cyclic voltammetry and rate performance measurements were carried out. The specific capacity measurement of $Li_2CoTi_3O_8$ obtained at 700 ºC is shown in Fig. 8. An initial discharge capacity of 82 mAh g^{-1} was found at 0.1 C for the $Li_2CoTi_3O_8/TiO_2$ nanoparticles and it dropped over 17% after 25 cycles following C-rates of 0.5, 1.0, 2.0, 4.0, and 0.1 C. The obtained results do not have a higher value than $LiCoO_2$ nanofibers. The decrement was as expected due to the loss of fiber network at high temperature calcination in the presence of TiO_2 nanoparticles. This result might be explained by the fact that 1D electrospun nanofibers

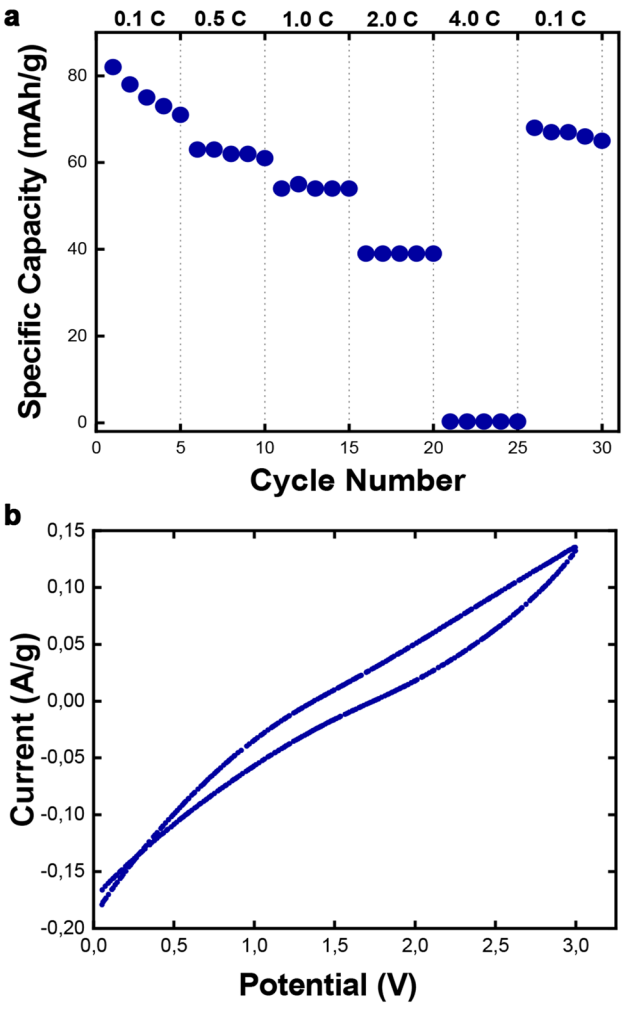

Fig. 8 **a** Rate performance and **b** Cyclic voltammogram of Li/$Li_2CoTi_3O_8/TiO_2$ coin cell battery ($Li_2CoTi_3O_8/TiO_2$ nanoparticles were fabricated at 700 ºC with a Li:Co mole ratio of 1:1)

compared to the nanoparticles have a larger surface area acting as a structural framework for the nanoparticles, hereby shorten the diffusion distance for lithium insertion, providing the electron conduction path along the fiber axis [43, 44]. It may be remarked that the cathode electrode was taken out from the coin cell after the rate performance tests for morphological observation, the $LiCoO_2$ nanofibers still preserved their continuous structure (Fig. S3). CV curves were measured between 0.01 and 3.00 V at a scan rate of 0.1 mV/s. There is no prominent peak which indicates the Li^+ insertion/extraction into the nanostructure. These results explain the low capacity which can be interpreted as the limitation arising from irreversible intercalation of the Li-ions into the stable $Li_2CoTi_3O_8$ structure.

When the battery performances of both $LiCoO_2$ and $Li_2CoTi_3O_8/TiO_2$ nanostructures are evaluated, compared to the conventional microparticle-based electrodes, they have low cycle stability and volumetric density because of their larger surface area with high porosity. Thus, they have large contact areas between the electrode and the electrolyte, which enhances the irreversible reaction [45–47].

4 Conclusion

In this study, we have fabricated electrospun $LiCoO_2$ and colloidal titania nanoparticles (TiO_2 NPs)-doped $LiCoO_2$ nanofibers as cathode electrodes in lithium-ion batteries. The increment in the calcination temperature and Li:Co mole ratio provides a lower capacity loss and higher performance of the battery. Furthermore, while the crystallinity and stability of the $LiCoO_2$ phase are improved, the presence of the TiO_2 NPs causes a transformation of binary $LiCoO_2$ to ternary Li-based transition metal oxide, $Li_2CoTi_3O_8$. It can be concluded that the synthesis parameters affect the structural characteristics of the $LiCoO_2$ and $Li_2CoTi_3O_8/TiO_2$ nanostructures and consequently, the change in their size, porosity, surface area, and geometry have a strong impact on battery performance. Therefore, new electrode materials, particularly Li-rich layered oxide nanomaterials, for high energy density and long cycle life batteries need to be developed for the requirement of intensive power sources through the continually growing energy markets.

Acknowledgements The authors gratefully acknowledge the financial support from the Izmir Katip Celebi University Scientific Research Project 2014-1-MÜH-15. The authors also thank Dr. Davut Uzun for the electrochemical measurements. Iztech Center for Materials Research is also acknowledged for SEM micrographs.

References

1. H. Li, Z. Wang, L. Chen, X. Huang, Adv. Mater. **21**, 45 (2009)
2. H. Wang, H. Dai, Chem. Soc. Rev. **42**, 7 (2013)
3. J.-W. Jung, C.-L. Lee, S. Yu, I.-D. Kim, J. Mater. Chem. A **4**, 3 (2016)
4. R. Yazami, *Nanomaterials for lithium-ion batteries: fundamentals and applications*, 1st edn. (Jenny Stanford Publishing, New York, 2013), pp. 139–165
5. A. Shukla, T.P. Kumar, Curr. Sci. **94**, 3 (2008)
6. N. Nitta, F. Wu, J.T. Lee, G. Yushin, Mater. Today **18**, 5 (2015)
7. Y.G. Guo, J.S. Hu, L.J. Wan, Adv. Mater. **20**, 15 (2008)
8. X. Kong, R. Zhou, J. Wang, J. Zhao, A.C.S. Appl, Energy Mater. **2**, 7 (2019)
9. L. de Biasi, A. Schiele, M. Roca-Ayats, G. Garcia, T. Brezesinski, P. Hartmann, J. Janek, Chemsuschem **12**, 10 (2019)
10. M.M. Thackeray, S.-H. Kang, C.S. Johnson, J.T. Vaughey, R. Benedek, S. Hackney, J. Mater. Chem. **17**, 30 (2007)
11. M. Büyükyazi, S. Mathur, Nano Energy **13**, 28–35 (2015)
12. G.-N. Zhu, Y.-G. Wang, Y.-Y. Xia, Energy Environ. Sci. **5**, 5 (2012)
13. J. Liu, X. Wei, F. Meng, *Advanced battery materials*, 1st edn. (Wiley VCH, Weinheim, 2019), pp. 87–157
14. Y. Wang, G. Cao, Adv. Mater. **20**, 12 (2008)
15. Y. Tang, L. Yang, Z. Qiu, J.S. Huang, Electrochem. Commun. **10**, 10 (2008)
16. H. Kawai, M. Tabuchi, M. Nagata, H. Tukamoto, A.R. West, J. Mater. Chem. **8**, 5 (1998)
17. Z. Liu, X. Zhou, *Graphene: energy storage and conversion applications* (CRC Press, Boca Raton, 2014), pp. 65–13
18. J.-G. Kim, D. Shi, K.-J. Kong, Y.-U. Heo, J.H. Kim, M.R. Jo, Y.C. Lee, Y.-M. Kang, S.X. Dou, A.C.S. Appl, Mater. Interfaces **5**, 3 (2013)
19. S.Y. Liu, C.Y. Fan, H.C. Wang, J.P. Zhang, X.L. Wu, Chem. Eur. J. **23**, 36 (2017)
20. D.H. Doughty, E.P. Roth, Electrochem. Soc. Interface **21**, 2 (2012)
21. Y. Gu, D. Chen, X. Jiao, J. Phys. Chem. B **109**, 38 (2005)
22. X. Zhang, L. Ji, O. Toprakci, Y. Liang, M. Alcoutlabi, Polym. Rev. **51**, 3 (2011)
23. A.F. Ismail, N. Hilal, J. Jaafar, C. Wright, *Nanofiber membranes for medical, environmental, and energy applications* (CRC Press, Boca Raton, 2019), pp. 215–235
24. W. Chee, H. Lim, Z. Zainal, I. Harrison, N. Huang, Y. Andou, K. Chong, A. Pandikumar, RSC Adv. **7**, 20 (2017)
25. S. Santangelo, Appl. Sci. **9**, 6 (2019)
26. C.T. Lim, Prog. Polym. Sci. **70**, 1–17 (2017)
27. X. Shi, W. Zhou, D. Ma, Q. Ma, D. Bridges, Y. Ma, A. Hu, J. Nanomater. **16**, 1 (2015)
28. N. Horzum, R. Muñoz-Espí, G. Glasser, M.M. Demir, K. Landfester, D. Crespy, A.C.S. Appl, Mater. Interfaces **4**, 11 (2012)
29. N. Sebastian, B. George, B. Mathew, Polym. Degrad. Stab. **60**, 2–3 (1998)
30. B. Jaquet, D. Wei, B. Reck, F. Reinhold, X. Zhang, H. Wu, M. Morbidelli, Colloid Polym. Sci. **291**, 7 (2013)
31. L. Li, Y.-L. Hsieh, Polymer **46**, 14 (2005)
32. S.A. Simakov, Y. Tsur, J. Nanopart. Res. **9**, 3 (2007)
33. N. Daels, M. Radoicic, M. Radetic, S.W. Van Hulle, K. De Clerck, Sep. Purif. Technol. **133**, 282e290 (2014)
34. M. Catauro, E. Tranquillo, G. Dal Poggetto, M. Pasquali, A. Dell'Era, S. Vecchio Ciprioti, Materials **11**, 12 (2018)
35. M. Krissanasaeranee, T. Vongsetskul, R. Rangkupan, P. Supaphol, S. Wongkasemjit, J. Am. Ceram. Soc. **91**, 9 (2008)
36. J.I. Langford, A. Wilson, J. Appl. Crystallogr. **11**, 2 (1978)
37. J. Wang, H. Zhao, Y. Shen, Z. Du, X. Chen, Q. Xia, ChemPlusChem **78**, 12 (2013)
38. S. Pinilla, A. Machín, S.-H. Park, J.C. Arango, V. Nicolosi, F. Márquez-Linares, C. Morant, J. Phys. Chem. B **122**, 2 (2017)
39. G. Ning, B. Haran, B.N. Popov, J. Power Sour. **117**, 160–169 (2003)

40. T.-F. Yi, Y. Xie, J. Shu, Z. Wang, C.-B. Yue, R.-S. Zhu, H.-B. Qiao, J. Electrochem. Soc. **158**, 3 (2011)
41. Y. Ou, J. Wen, H. Xu, S. Xie, J. Li, J. Phys. Chem. Solids **74**, 322–327 (2013)
42. Y. Mizuno, E. Hosono, T. Saito, M. Okubo, D. Nishio-Hamane, K. Oh-ishi, T. Kudo, H. Zhou, J. Phys. Chem. C **116**, 19 (2012)
43. H.G. Wang, S. Yuan, D.L. Ma, X.B. Zhang, J.M. Yan, Energy Environ. Sci. **8**, 1660–1681 (2015)
44. Z. Hong, X. Zheng, X. Ding, L. Jiang, M. Wie, and K. Wie, Energy Environ. Sci. 4 (2011)
45. Y. Yu, Y. Liu, X. Yang, in *Alkali-Ion Batteries*, ed. by D. Yang (IntechOpen, London, 2016), pp. 111–125
46. C. Daniel, D. Mohanty, J. Li, D.L. Wood, AIP Conf. Proc. **1597**, 26 (2014)
47. X. Feng, *Nanocarbons for Advanced Energy Storage* (Wiley, Hoboken, 2015), pp. 59–87